Origin of gradients in lipid density and surface tension between connected lipid droplet and bilayer

Abdou Rachid Thiam, Aymeric Chorlay, Lionel Forêt

Origin of gradients in lipid density and surface tension between connected lipid droplet and bilayer

Aymeric Chorlay[1], Lionel Forêt[1,*], Abdou Rachid Thiam[1*]

[1] Laboratoire de Physique de l'École Normale Supérieure, ENS, Université PSL, CNRS, Sorbonne Université, Université de Paris, F-75005 Paris, France

***Correspondence to**:
Lionel foret
lionel.foret@phys.ens.fr
or
Abdou Rachid Thiam
thiam@ens.fr

Laboratoire de Physique,
Ecole Normale Supérieure,
PSL Research University,
75005 Paris Cedex 05, France

Abstract.

We combined theory and experiments to depict physical parameters modulating the phospholipid (PL) density and tension equilibrium between a bilayer and an oil droplet in contiguity. This situation is encountered during a neutral lipid (NL) droplet formation in the endoplasmic reticulum. We set up macroscopic and microscopic models to uncover free parameters and the origin of molecular interactions controlling the PL densities of the droplet monolayer and the bilayer. The established physical laws and predictions agreed with experiments performed with droplet-embedded vesicles. We found that the droplet monolayer is always by a few percent (~10%) less packed with PLs than the bilayer. Such a density gradient arises from PL-NL interactions on the droplet, which are lower than PL-PL trans-interactions in the bilayer, i.e., interactions between PLs belonging to different leaflets of the bilayer. Finally, despite the pseudo-surface tension for the water/PL acyl chains in the bilayer being higher than the water/NL surface tension, the droplet monolayer always has a higher surface tension than the bilayer because of its lower PL density. Thus, a PL density gradient is mandatory to maintain the mechanical and thermodynamic equilibrium of the droplet-bilayer continuity. Our study sheds light on the origin of the molecular interactions responsible for the unique surface properties of lipid droplets compared to cellular bilayer membranes.

Significance.

Organelles' biogenesis and function rely on membrane mechanics and phospholipid composition. Lipid droplets (LDs) are unique cell organelles because of their neutral lipid oil core shielded by a single phospholipid monolayer. LD biogenesis happens in the endoplasmic reticulum (ER) bilayer, which unzips to encapsulate the developing LD that subsequently buds off in the cytoplasm. The ER cytoplasmic monolayer leaflet thus equilibrates with that of the forming LD. Experimental data and simulations support that this equilibration happens with different phospholipid densities and tensions between the bilayer and monolayer, but the underlining mechanisms remain unknown. A theoretical framework combined with experiments enabled us to reveal these mechanisms.

Introduction.

Except for lipid droplets (LDs), most cellular organelles are bilayer bounded (1). LDs are made of neutral lipids, which are non-membrane lipids and often oily molecules. These neutral lipids are encapsulated in the core of the LDs, covered by a single phospholipid monolayer in which proteins are embedded. LD forms in the ER bilayer following a multiple steps process (2, 3). Neutral lipids are synthesized and sheltered in the ER bilayer's hydrophobic region. The neutral lipids phase separates from the ER bilayer at a critical concentration and condenses into an LD (4–6). At this stage, the LD is contiguous with the ER bilayer and can exchange proteins and lipids with its membrane (7). The nucleated LDs grow by acquiring more neutral lipids and proteins. At maturation, LDs can be physically disconnected from the ER bilayer but may reconnect with it later to exchange content (8, 9). Hence, the droplet monolayer surface is functionally connected to the ER bilayer to maintain the homeostasis of lipids and proteins of the LDs (10–12). A crucial question is how these organelles manage to share phospholipids and proteins while keeping their respective identity. Answering this question will help understand LD biogenesis and protein targeting principles (13–17). In particular, understanding how the density of phospholipids is set between contiguous bilayer and monolayer interfaces will allow better knowing mechanisms of LD assembly and protein binding (13, 16–18).

Important parameters controlling LD biogenesis are the monolayer and bilayer surface tension and curvature (19–21), which depend on the phospholipid composition of the organelles (16, 22, 23). The phospholipid density regulates both the LD monolayer surface tension and its accessibility to proteins (8, 16, 24–28). Firstly, while the ER bilayer can behave as an infinite phospholipid reservoir to the connected LD, reconstitution approaches, cell data, and molecular dynamics simulations suggest that the droplet monolayer is less packed with phospholipids than the ER bilayer (25, 29–31). Such a discrepancy partly explains the higher recruitment of peripheral or monotopic membrane proteins to LDs than bilayer membranes (24, 25, 30, 32, 33). Secondly, while the ER bilayer is of low surface tension, circa 0.01mN/m (34), cellular LDs, made from and contiguous with the ER, have a surface tension above 1mN/m (19, 20), two orders of magnitudes higher. This tension difference is crucial for the proper emergence of LDs from the ER bilayer (16, 17, 19). Reasons for the discrepancies in phospholipid densities and surface tensions between LDs and the ER bilayer are unclear as yet. Understanding the molecular basis of such differences between the two contiguous organelles will improve our knowledge of their biology.

Whether the physical properties of phospholipid bilayers and monolayers are identical was raised several decades ago (35–37) because both are self-assembled interfaces with essential functions and applications in biology and physical science. For example, early studies focused on the kinetics and mechanics of the phospholipid monolayers of air/water or water/oil interfaces for better understanding the dynamics of lung surfactants (38) or emulsions' stability for digestion purposes (32, 33), etc. In the meantime, biophysical approaches allowed studying the mechanics and dynamics of phospholipid bilayers, an important branch of membrane biology (41–43). Altogether, these pioneer focuses on phospholipid interfaces led to the genesis of several theoretical frameworks describing the mechanics and thermodynamics of phospholipid-coated fluid interfaces (35, 36, 44). However, because LDs have

gained focus relatively lately, little or no application was devoted to studying the case of the phospholipid monolayer interface covering an LD emerging from the ER bilayer. Mechanisms controlling the phospholipid density and surface tension equilibrium between a droplet monolayer jointed to a bilayer are currently unknown. We decided to capitalize on the established theoretical frameworks to uncover them.

This paper aims to unveil the molecular origin of mechanisms maintaining the uneven phospholipid density between a droplet monolayer connected to a bilayer (Figure 1A). We customized macroscopic and microscopic frameworks of such a situation and established the relationship between the free parameters of the system.

Experiments validated our theoretical predictions, and this agreement allowed us to highlight molecular interactions underlying the difference in phospholipid densities and surface tensions between the droplet monolayer and bilayer. These interactions involve (a) the adhesion between the phospholipid monolayer leaflets forming the bilayer, which does not exist on a droplet monolayer, and (b) a pseudo-surface tension –resulting from the interaction between water molecules and phospholipid acyl chains of the bilayer– higher than the classical water/oil surface tensions. Keeping a phospholipid density difference is essential for the mechanical and thermodynamic equilibrium of the droplet and bilayer contiguity.

Results.

The result section is organized as follow. We first present the thermodynamic equilibrium relations, which govern the droplet morphology and the phospholipid distribution between the droplet monolayer interfaces and the bilayer. In the second part, we analyze one important and experimentally testable consequence of the equilibrium conditions: the interdependence between the surface tensions of the droplet and the bilayer, which reflects the coupling between the monolayer and bilayer phospholipid densities. The theoretical predictions made from this second part are successfully verified experimentally in the third part. In the fourth part, we present a microscopic theoretical description of the contiguous monolayers and bilayer, enabling us to derive the state equations of these interfaces. These equations are then used to understand the molecular origin of the density difference (part five) and surface tension difference (part six) between the monolayers and the bilayer. In the last part, a quantitative comparison between theory and experiments is made to validate the theoretical approach and its underlying hypothesis.

Thermomechanical equilibrium of a lipid droplet connected to a phospholipid bilayer

We consider a droplet of fixed volume, above tens of nm in size, connected to a phospholipid (PL) bilayer (Figure 1A). At this scale, the contribution of the bending elasticity and long-range interactions of the different interfaces is negligible (17, 19). Hence, the PL bilayer and the droplet interfaces can be described as homogeneous fluid interfaces joining at the droplet edge (17). A line tension arises at this contact, but its contribution to the order of tens of pN is negligible with respect to surface tension forces (17) (Discussion of the origin and influence of the line tension in Supplement text sections 1 and 3). The free energy of the droplet embedded in a bilayer is then,

$$F = A_b f_b(\rho_{be}, \rho_{bi}) + A_{me} f_m(\rho_{me}) + A_{mi} f_m(\rho_{mi}), \quad (1)$$

where A_b, A_{me}, A_{mi} are the area of the three interfaces (bilayer and monolayers covering the LD at the "external" and "internal" side); $\rho_{be}, \rho_{bi}, \rho_{me}, \rho_{mi}$ are the PL surface density in each bilayer leaflet and each monolayer (Fig. 1C); f_b and f_m are the free energy per surface unit of a PL bilayer and a PL monolayer at the water/oil interface. (A more thorough discussion of the assumptions leading to equation (1) in Supplement text section 1). We consider that PLs freely diffuse and equilibrate between the droplet and the bilayer (Figure 1A). PL flip-flop, which takes several hours or days under passive conditions (45, 46), is much slower than the lateral diffusion of PLs (~μm^2/sec) (21) and is negligible at relevant time scales (Figure 1A). Also, experimentally, PLs are insoluble in the neutral lipid oil phase, which is why they self-assemble into droplet interface bilayers (19); therefore, PL exchange does not occur through the droplet in the relevant time scales. Under these conditions, the PL number of each leaflet is constant,

$$N_e = \rho_{me} A_{me} + \rho_{be} A_b = constant \quad \text{and} \quad N_i = \rho_{mi} A_{mi} + \rho_{bi} A_b = constant, \quad (2)$$

where N_e and N_i can be different.

At equilibrium, the morphology of the connected droplet and bilayer, as well as the distribution of PL between the droplet and the bilayer, minimize the free energy (equation (1)), under the constraints of equation (2) and of fixed droplet volume. This minimization yields the usual equilibrium conditions presented in the following.

The droplet and bilayer shapes obey the laws of three-fluid phase wetting systems (47). The interfaces must have a constant mean curvature (Laplace law). We focused on axisymmetric geometries for which the droplet interfaces are spherical caps, and the bilayer can either be flat or bear a constant curvature. The droplet morphology is fully characterized by the contact angles between the droplet interfaces and the bilayer, θ_e and θ_i (Figure 1B). These angles are fixed by the balance of the forces acting at the contact line (Figure 1B): $\vec{\gamma}_{me} + \vec{\gamma}_{mi} + \vec{\gamma}_b = 0$ or,

$$\gamma_{me}\cos\theta_e + \gamma_{mi}\cos\theta_i + \gamma_b = 0, \qquad \gamma_{me}\sin\theta_e = \gamma_{mi}\sin\theta_i\,, \tag{3}$$

where γ_{me}, γ_{mi}, γ_b are respectively the surface tension of the external and internal monolayers of the droplet (me, mi), and the bilayer (b). In vitro experiments (20) confirmed the validity of equation (3) to describe the morphology of large membrane-embedded droplets. In the particular case, where the bilayer is tensionless, $\gamma_b = 0$, the angles are not unequivocally determined but must be such that $\theta_e + \theta_i = 180°$, which implies that the droplet is spherical.

The PL partitioning between the bilayer and droplet monolayers (Figure 1C) is controlled by the chemical potentials equilibrium,

$$\mu_{me} = \mu_{be} \quad \text{and} \quad \mu_{mi} = \mu_{bi}\,, \tag{4}$$

where μ_{me}, μ_{mi}, μ_{be}, μ_{bi} respectively denote the chemical potential of the external and internal monolayers of either the droplet (me, mi) or the bilayer (be, bi). A monolayer and its contiguous bilayer leaflet have equal chemical potentials. Because of the rapid diffusion of PLs, the chemical potential equilibrium is quickly reached, much faster than the growth rate of a cellular LD (~minutes) or the time scale of perturbations imposed in droplet-embedded vesicles (16, 20).

Surface tensions and chemical potentials are functions of the PL densities: $\gamma_{me} = \gamma_m(\rho_{me})$, $\gamma_{mi} = \gamma_m(\rho_{mi})$, $\mu_{me} = \mu_m(\rho_{me})$, $\mu_{mi} = \mu_m(\rho_{mi})$, $\gamma_b(\rho_{be}, \rho_{bi})$, $\mu_{be} = \mu_b(\rho_{be}, \rho_{bi})$, $\mu_{bi} = \mu_b(\rho_{bi}, \rho_{be})$, where γ_m, μ_m, γ_b, μ_b can be expressed in terms of the free energy densities f_m and f_b defined in equation (1) and their derivatives, equations (MM1- MM3) (Materials and Methods). It follows that the relations (3) and (4) are interdependent: a variation in PL densities modulates tensions, which alter the contact angles (equation (3)) and interface areas, as the droplet volume is fixed. Conversely, changes in morphology, and, hence, in interfacial areas, redistribute PLs because of mass conservation (equation (2)) and, subsequently, modify chemical potentials (equation (4)).

In conclusion, for a given oil volume, number of PLs in each membrane leaflet and bilayer tension, the PL densities, ρ_{me}, ρ_{mi} , ρ_{be} , ρ_{bi}, and the contact angles, θ_e , θ_i, adjust in a coupled manner to fulfill the thermomechanical equilibrium conditions (equations (3), (4)).

Coupling between phospholipid densities and between surface tensions

The above equilibrium relations impose an interdependence between the different interfaces' PL density and, thus, the droplet and bilayer surface tensions via two distinct mechanisms.

The first coupling mechanism pertains to the chemical potential equilibriums, equation (4). Indeed, a slight variation in surface tension of one interface will modify the density of this interface. In response, PLs will redistribute between the adjacent interfaces to re-establish the equilibrium of the chemical potentials (equation (3)). Such an adjustment will change the respective PL densities and, hence, the surface tensions. The link between variations of surface tension and chemical potentials of an interface, due to variation of its PL density, is expressed by the Gibbs-Duhem relations,

$$d\gamma_m = -\rho_m d\mu_m \quad \text{and} \quad d\gamma_b = -\rho_{be} d\mu_{be} - \rho_{bi} d\mu_{bi} \,. \tag{5}$$

Combining these relations and the differentials of equation (4), $d\mu_{me} = d\mu_{be}$, $d\mu_{mi} = d\mu_{bi}$, we obtain a general link between surface tension variations,

$$d\gamma_b = \frac{\rho_{be}}{\rho_{me}} d\gamma_{me} + \frac{\rho_{bi}}{\rho_{mi}} d\gamma_{mi} \,. \tag{6}$$

This first coupling due to the chemical potential equilibrium (4) is the unique coupling in two practical and biologically interesting situations: a symmetrical bilayer and an infinite bilayer reservoir.

In a symmetrical membrane, $\rho_{be} = \rho_{bi} = \rho_b$ and $\rho_{me} = \rho_{mi} = \rho_m$, the balance of chemical potentials (equation (4)) reads $\mu_m(\rho_m) = \mu_b(\rho_b)$ and therefore imposes an unequivocal relation between bilayer and monolayer tensions, $\gamma_b(\rho_b)$ and $\gamma_m(\rho_m)$. Thereupon, equation (6) becomes,

$$d\gamma_m = \frac{1}{2}\frac{\rho_m}{\rho_b} d\gamma_b \tag{7}$$

This relation indicates that the droplet interfacial tension increases with the bilayer one with a slope proportional to the ratio of their PL densities.

For a droplet embedded in a large ($A_b \gg A_{me,mi}$) and possibly asymmetrical membrane, the bilayer behaves as an infinite PL reservoir of fixed PL density, independent of the state of the droplet. This configuration is more relevant in cell conditions when nascent LDs form in the ER membrane. In this case, a similar relation as equation (7) holds,

$$d\gamma_{me} = \beta_e \frac{\rho_{me}}{\rho_{be}} d\gamma_b \quad (8)$$

and $d\gamma_{mi} = \beta_i \frac{\rho_{mi}}{\rho_{bi}} d\gamma_b$ with $\beta_i = 1 - \beta_e$ (derivation of equation (8) and definition of β_e in Supplement text, section 6.3). This equation shows that the monolayer tension should also increase linearly with the bilayer ones as for a symmetrical membrane, but with a numerical pre-factor depending on the membrane asymmetry; $\beta_e > 1/2$ if the external leaflet is less dense than the internal one and vice-versa.

A second density coupling mechanism exists for small (bilayer area comparable to droplet area) and asymmetrical membranes. This coupling arises from the PL number conservation (equation (2)) and the mechanical equilibrium (equation (3)), together linking the PL distribution to the system's morphology. A change in surface tension affects the morphology (equation (3)), i.e., the surface area of the interfaces, which in turn impacts the densities (equation (2)), and hence tensions. No simple mathematical relations resembling equation (6) expressing this coupling can be derived.

Experimental determination of the interdependence between surface tensions

We wanted to experimentally test the theoretical findings by probing the interdependence between the droplet and bilayer surface tensions. For this purpose, we used the droplet-embedded vesicle system (DEV) (19, 48) (Figure 2A), which mimics the theoretically described situation of an oil droplet in contiguity with a bilayer. DEVs were formed by inserting triolein droplets within the bilayer of giant unilamellar vesicles made of DOPC (1,2-dioleyl-sn-3glycero-3-phosphocholine) (48).

The external droplet monolayer and the bilayer of the DEV were captured by two micropipettes (Figure 2B). We selected DEVs with a symmetrically positioned droplet, *i.e.,* identical contact angles $\theta_e = \theta_i$, which, consequently, have similar tension, $\gamma_{me} = \gamma_{mi}$ (equation (3)). These DEVs meet the symmetric condition leading to equation (7), which can be tested experimentally. To establish the tension dependency predicted by this equation, we imposed the DEV bilayer tension step by step, by fixing the aspiration pressure of the micropipette, and concomitantly measured the micropipette-aspiration-applied surface tension of the external monolayer of the droplet (Figure 2B). We found that the monolayer tension increased with the bilayer tension (Figure 2C), agreeing with the theoretical description: increasing the bilayer tension decreases the chemical potential in the bilayer leaflets; to keep the chemical potential equilibrium, the droplet must, therefore, supply PLs to the bilayer, resulting in its tension increase.

Interestingly, the tensions' dependency followed a linear trend line (Figure 2C). Based on equation (7), this linear dependency suggests that the ratio of the monolayer-to-bilayer PL density did not vary, independently of the bilayer tension. The slope $\frac{\rho_m}{2\rho_b}$ of 0.45±0.02, indicates that the bilayer PL density is slightly higher than the monolayer one, agreeing with our previous fluorescence and droplet tensiometer measurements where this value was of 0.435 (30).

The PL density is maximum, i.e., close to full packing, in a tensionless bilayer. Since the droplet monolayer PL density evolves like the bilayer one, one may speculate that it also reaches near close packing when the bilayer is tensionless. Thereupon, the monolayer tension would also be close to zero. Such assumption was not valid as, when the bilayer tension fell to almost zero (<0.01 mN/m), the monolayer tension was non-negligible, around 1.5 mN/m (Figure 2C). We initially hypothesized that the non-zero tension of the monolayer could be due to the nature of the tensionless bilayer of the DEV, which may have been unable to supply PLs to the droplet. To test this hypothesis, we changed the system and put the droplet in contact with another type of PL reservoir.

At the tip of a tensiometer apparatus, we generated a triolein oil-in-buffer droplet, over-supplied with PLs in the oil (0.5% w/w to triolein) (Figure 2D, left). In this setting, the oil phase acts as a PL reservoir to the droplet interface. As soon as the droplet was formed in the buffer solution, the surface tension dropped down, due to the spontaneous adsorption of PLs to the interface, to reach an equilibrium value of 1.15 mN/m (Figure 2D, Figure S1D); without PLs, the triolein/buffer tension is ~34 mN/m. Thus, even with this reservoir, the monolayer tension was non-zero and close to the ~1.5 mN/m obtained with DEV (Figure 2C). Next, starting from the equilibrium tension at 1.15mN/m, we mechanically compressed the PL monolayer of the droplet by sucking off the droplet volume (Figure 2D, Figure S1E). Even under this action, surface tension decreased but was still not close to zero, ~0.6 mN/m, compared with the tensionless bilayer (<0.01 mN/m). These results indicate that, unlike a bilayer, a droplet monolayer has specific features, detailed hereafter, that prevent it from reaching a high PL density and near-zero surface tension.

Altogether, the experiments with DEVs are consistent with the theoretical prediction (equation (7)). For symmetrical conditions, the monolayer tension responds linearly to an increase in bilayer tension, implying that the phospholipid density ratio is constant between the bilayer and the monolayer. However, our results revealed two essential aspects: (i) through the bilayer and the droplet are connected, the PL density is lower for the droplet monolayer than the bilayer, and (ii) the tensions of the droplet and the bilayer are largely different in general; even in contact with a bilayer of very low tension, the droplet remains at relatively high tension (above 1 mN/m). In the following sections, we delve deeper into these findings with a theoretical approach, subsequently validated by a quantitative analysis of the surface tensions curves of DEVs.

Microscopic description of the contiguous droplet-bilayer system

To pinpoint the origin of the molecular interactions responsible for the discrepancy in tension and PL density between the monolayer and bilayer, we developed a microscopic description closely following the approach and assumptions of refs. (36, 44). The goal is to express the equations of state relating surface tensions, chemical potentials, and densities, for a monolayer and a bilayer.

The different contributions to the free energy of a monolayer and a bilayer are depicted in (Figure 3A). The free energy per surface unit of a monolayer at a water/oil interface function of the PL density can be written as,

$$f_m(\rho) = \gamma_{o/w} + f_{\mathrm{int}}(\rho) + f_{\mathrm{hyd}}(\rho) + f_{\mathrm{mo}}(\rho)\,. \tag{9}$$

The four terms account respectively for the bare oil/water surface tension, lateral PL - PL interactions, hydrophilic interaction of PL head groups with water, PL tails interaction with oil. The free energy density of the bilayer is,

$$f_b(\rho_{be}, \rho_{bi}) = f_{\mathrm{int}}(\rho_{be}) + f_{\mathrm{hyd}}(\rho_{be}) + f_{\mathrm{phob}}(\rho_{be}) + f_{\mathrm{int}}(\rho_{bi}) + f_{\mathrm{hyd}}(\rho_{bi}) + f_{\mathrm{phob}}(\rho_{bi}) + f_{\mathrm{mm}}(\rho_{be}, \rho_{bi})\,. \tag{10}$$

The functions f_{int} and f_{hyd} in equation (10), which account for the lateral interactions between PLs and from PL head – water in a bilayer leaflet, are identical to the ones in equation (9) for the monolayer. The term f_{mm} accounts for the *trans* interaction between the two leaflets, *i.e.,* the interaction between the tails of PLs belonging to different leaflets. Lastly, f_{phob} accounts for the hydrophobic interaction of PL tails with water, responsible for the cohesion of bilayer in water. Following ref. (37), this contribution is supposed to be negligible for monolayer (and is thus absent in equation (9)) and nearly constant $f_{\mathrm{phob}}(\rho) = \gamma_{\mathrm{phob}}$ for bilayer, with the parameter γ_{phob} of the order 34 to 39 mN/m for DOPC. The contributions f_{mo} and f_{mm} are assumed to be linear in PL densities (37), $f_{\mathrm{mo}}(\rho) = \varepsilon_{\mathrm{mo}}\rho$ and $f_{\mathrm{mm}}(\rho_{be}, \rho_{bi}) = \varepsilon_{\mathrm{mo}}(\rho_{be} + \rho_{bi})$, *i.e.*, the free energy per PL molecule due to PL tail interaction (with oil in a monolayer and with the tails of PL in the other leaflet in a bilayer), $\varepsilon_{\mathrm{mo}}$ and $\varepsilon_{\mathrm{mm}}$ are constant parameters.

The surface tension and the chemical potential of a monolayer, functions of the PL density, can be deduced from the free energy equation (9) and equation (MM1) (material and method):

$$\gamma_m(\rho) = \gamma_{o/w} - \pi(\rho) \tag{11}$$

and

$$\mu_m(\rho) = \int \frac{\pi'(\rho)}{\rho} d\rho + \varepsilon_{\mathrm{mo}}\ , \tag{12}$$

where the prime denotes the derivative of the function. The quantity $\pi(\rho)$, named the lateral pressure, is defined as $\pi(\rho) = \rho\left(f_{\mathrm{int}}'(\rho) + f_{\mathrm{hyd}}'(\rho)\right) - f_{\mathrm{int}}(\rho) - f_{\mathrm{hyd}}(\rho)$: it arises from lateral PL - PL interactions and hydrophilic PL head interactions. This lateral pressure can be measured and well described theoretically by classical equations of state of two-dimensional fluids, such as the van der Waals equation of state (37), see below.

The surface tension of a bilayer function and the chemical potential of one of its leaflets, functions of the leaflet densities, are deduced from equation (10) and equations (MM2-MM3) (Materials and Method), and read,

$$\gamma_b(\rho_{be}, \rho_{bi}) = 2\gamma_{\mathrm{phob}} - \pi(\rho_{be}) - \pi(\rho_{bi}) \quad (13)$$

and

$$\mu_b(\rho_b) = \mu_m(\rho_b) + \varepsilon_{\mathrm{mm}} - \varepsilon_{\mathrm{mo}} \quad . \quad (14)$$

(The chemical potential of a leaflet is independent of the density of the other leaflet under our assumptions.)

A central parameter in these state equations (11 – 14) is the lateral pressure $\pi(\rho)$. By using the pending drop experiment, described Fig. 2C and ref. (30), we obtained $\pi(\rho)$ for a DOPC monolayer at the water – TO interface (Figure 3B, Figure S2A); it was well described by a van der Waals state equation, $\pi(\rho) = \frac{kT\rho}{1-a\rho} - u\rho^2$. The parameter a characterizes the excluded area due to steric repulsion and u the strength of the lateral interactions between PL molecules (Materials and Methods, Figure S2B). The determination of $\pi(\rho)$ enabled us to determine (up to a constant) $\mu_m(\rho)$ using equation (12) (Figure 3C). Note that the exact profile of $\pi(\rho)$ depends on the PL type, yet the global features of the curves in Fig. 3B and C should be generic.

Combining the state equations (11 - 14) with the equilibrium conditions (4), we discuss in the following two sections the origin of the density difference between the connected monolayers and bilayer, and then the basis of their surface tension difference. Additionally, these equations of state allow performing a complete quantitative analysis of the surface tension curves obtained for DEVs, in particular in the case of asymmetric DEVs (last section).

Droplet-bilayer phospholipid equilibration following the microscopic description

PL partitioning is governed by the equilibrium condition (4): the PL densities in adjacent monolayer and bilayer leaflet, ρ_m and ρ_b, are such that $\mu_m(\rho_m) = \mu_b(\rho_b)$. The chemical potentials of the monolayer and bilayer leaflet, μ_b and μ_m, functions of the PL density, as given by the state equations (12) and (14), are shown in Figure 3C. The two curves have the same profiles, but are shifted by $\varepsilon_{\mathrm{mm}} - \varepsilon_{\mathrm{mo}}$. Then, for the chemical potentials to be equal, the densities of contiguous monolayer and bilayer must be different in general, $\rho_m \neq \rho_b$, as long as $\varepsilon_{\mathrm{mm}} \neq \varepsilon_{\mathrm{mo}}$. Thereupon, the microscopic description (equation (14)) pinpoints the parameter $\varepsilon_{\mathrm{mm}} - \varepsilon_{\mathrm{mo}}$ as the primary lever imposing the phospholipid density difference between the monolayer and bilayer. We remind that this parameter quantifies the difference in interactions of PL tails with their underneath environments which are: the tails of PLs in the opposite leaflet for the bilayer, and the NL oil phase for the droplet monolayer (Figure 3A). Depending on the sign of $\varepsilon_{\mathrm{mm}} - \varepsilon_{\mathrm{mo}}$, the monolayer lipid density is always larger or smaller than the bilayer leaflet density.

However, according to the surface tension measurements (Figure 2C) and equation (5), the PL density is expected to be lower at the droplet interface $\rho_m < \rho_b$, meaning that $\varepsilon_{\mathrm{mm}} - \varepsilon_{\mathrm{mo}} < 0$. Consequently, trans-interactions between PL tails in the bilayer are energetically more favorable than the interactions of PL tails with oil molecules in the droplet.

Assuming a slight relative difference of PL density between the droplet monolayer and bilayer leaflet, and expanding the equilibrium relation $\mu_b(\rho_b) = \mu_m(\rho_m)$ to the linear order (Supplement text, section 8), one obtains

$$\frac{\rho_b - \rho_m}{\rho_b} \simeq \frac{\varepsilon_{\mathrm{mo}} - \varepsilon_{\mathrm{mm}}}{\pi'(\rho_b)} \qquad (15)$$

This equation shows that the relative density difference between the bilayer and droplet monolayer is modulated by $\varepsilon_{\mathrm{mm}} - \varepsilon_{\mathrm{mo}}$ (Figure 3A). A bilayer is stable only in a narrow range of PL density, near close packing, and can be stretched by only about 5% (49, 50). Consequently, $\pi'(\rho_b)$ should be very large and, according to equation (15), the relative difference in density between a bilayer leaflet and its contiguous droplet monolayer should be relatively small. This interpretation agrees with the density ratio obtained from the slope of Figure 2C using equation (7) and our recent experimental finding in DEVs (30), suggesting that for 100 PLs on a bilayer leaflet, droplet monolayer in contiguity with this leaflet has ~90 PLs.

Surface tensions comparison following the microscopic description

Combining the previous results on the PL distribution with the state equations (11, 13) allows understanding how the droplet tension compares with the bilayer one. In particular, we wanted to understand why the droplet remains with a non-zero tension while being in contact with a tensionless bilayer (Figure 2C).

According to equation (11), the droplet surface tension is maximal in the absence of PLs, equal to $\gamma_{o/w}$, and decreases when the PL density or the lateral pressure increases. The bilayer tension has a similar dependency on the PL density (equation 13), with γ_{phob} being reminiscent of $\gamma_{o/w}$, though they have different molecular origins (Figure 3A). As found above, the bilayer PL density should always be slightly higher than the droplet monolayer one. Consequently, the monolayer should be of lower lateral pressure than the bilayer leaflet, i.e., $\pi(\rho_b) > \pi(\rho_m)$.

At zero bilayer tension, the mechanical equilibrium condition (3) imposes the same tension and thus the same PL densities between the two droplet monolayers. It follows from equation (4) that the two bilayer leaflets also have the same density, ρ_b^0. Under this condition, the lateral pressure in the bilayer balances exactly the hydrophobic contribution in equation (11), $\gamma_{\mathrm{phob}} = \pi(\rho_b^0)$. On the droplet monolayer side, the lateral pressure is lower, i.e., $\pi(\rho_m^0) < \pi(\rho_b^0)$, and too small to completely cancel the tension of the droplet interface (equation (10)), $\gamma_m^0 = \gamma_{o/w} - \pi(\rho_m^0) \neq 0$. Assuming a slight relative difference in PL density between a monolayer and a bilayer leaflet (30), the tension of a droplet embedded in a tensionless bilayer can be approximately expressed by (Supplement text, section 8),

$$\gamma_m^0 \simeq \gamma_{o/w} - \gamma_{\mathrm{phob}} + \rho_b^0(\varepsilon_{\mathrm{mo}} - \varepsilon_{\mathrm{mm}}) \quad (16)$$

This equation shows that $\gamma_{o/w} - \gamma_{\mathrm{phob}}$ and $\varepsilon_{\mathrm{mo}} - \varepsilon_{\mathrm{mm}}$, which controls the monolayer-bilayer density mismatch, are the two key parameters keeping the droplet monolayer tension to a non-zero value when the bilayer is tension-free.

The parameters $\gamma_{o/w}$ and $\varepsilon_{\mathrm{mo}}$, are a function of the oil type. Thus, changing the oil type should vary the tension of the droplet when the bilayer is tensionless (equation (11)). To test this prediction, we established the monolayer-bilayer tension diagram of DEVs made with different oils. Namely, we used a triolein-sterol ester mixture or squalene (Figure 3D-E). Independently of the oil type, a linear trend was observed for symmetric DEVs, as expected from equation (7). The slopes were also conserved, confirming that these oils' monolayer-bilayer densities were similar (30). However, the droplet tension at zero bilayer tension was significantly different (Figure 3E), agreeing with our prediction from the theoretical analysis (equation (16)). At very low bilayer tension (<0.1mN/m), the squalene droplet had a lower tension than the triolein one (Figure 3E). Since $\gamma_{o/w}$ was respectively 23.7 mN/m and 34 mN/m for squalene and triolein, the term $|\gamma_{o/w} - \gamma_{\mathrm{phob}}|$ would be lower for squalene, which, following equation (16), would partly explain the lower droplet monolayer tension value for squalene.

Validation of the microscopic model by the quantitative analysis of the DEV system

We wished to compare quantitatively experimental data obtained with the DEV system and theory output to go beyond the qualitative agreement between theoretical predictions and experimental observations. A quantitative agreement would eventually validate our theoretical approach and the underlying hypothesis.

We built a complete theoretical description of the DEV system based on the thermodynamic approach developed in the preceding sections (Supplementary text, section 7). The model allows us to compute all the characteristics of a DEV, in particular the surface tension of the different interfaces, which are experimentally measurable and tunable observables. The parameters of the model are of two origins: geometrical and physicochemical. The geometrical parameters (oil volume, vesicle inner volume and leaflet asymmetry in PL number) are specific to each DEV and are experimentally obtained by image analysis. The physicochemical (or microscopic) parameters are the ones in the state equations (11-14) and only depend on the PL and oil types composing the DEV. The physicochemical parameters $\gamma_{o/w}$ and the lateral pressure were determined by the drop tensiometer method (Figure S2B). The only unknown physicochemical parameters of the model are hence γ_{phob} and $\varepsilon_{\mathrm{mo}} - \varepsilon_{\mathrm{mm}}$ (Figure 3A). We adjusted these two parameters to fit the model to the surface tensions data of Figure 2C, obtained with a symmetric DEV. We found that $\gamma_{\mathrm{phob}} = 38.6$ mN/m, close to reported values for DOPC (36), and $\varepsilon_{\mathrm{mm}} - \varepsilon_{\mathrm{mo}} = -4.4$ pN.nm $= 1.1\, k_B T$ (Table Figure 4B). The value of $\varepsilon_{\mathrm{mm}} - \varepsilon_{\mathrm{mo}}$, looks rather low but sufficient enough to proffer a higher PL packing to the bilayer than the monolayer (equation (14)). This means that the small differences between the PL tail - NL interactions on the droplet and the tail-tail

interactions between PLs on opposite leaflets of the bilayer are sufficient to induce a PL density gradient between the bilayer and the monolayer.

By definition, the above values of the different physicochemical (or microscopic) parameters should only be set by molecular interactions, exclusively depending on the PL and oil type and not on DEV geometry. Therefore, the values of these parameters should allow fitting the model for any DEV geometry. To test this prediction, we considered DEVs, made of DOPC vesicles and triolein droplets of different sizes, and different asymmetries in DOPC number between their internal and external leaflets. PL asymmetry is obvious at low bilayer tension, as the droplets are spherical (16, 20) and differently positioned in the bilayer (16, 20): the droplets are either centered, $\theta_e = \pi/2$, or emerged outward, $\theta_e < \pi/2$, or inward, $\theta_e > \pi/2$, (Figure 4A, Figure S3 A-D). We took advantage of this variability in DEV geometry, i.e., in size and asymmetry, to test whether the microscopic parameters' values (Table Figure 4B) allow us to predict the correct DEVs tensions for all DEV geometry.

For each DEV (Figure S3 A-D), including the one in Figure 2C, we measured the tension of the external droplet monolayer γ_{me} against the bilayer one γ_b (Figure 4A, data points); we also determined by image analysis the DEV geometrical parameters (size and droplet position asymmetry). Then, using the microscopic parameters' values (Table Figure 4B), we computed γ_{me} as a function of γ_b for each DEV imposing specific geometrical constraints (Figure 4A, model, solid lines). Strikingly, the computed curves were perfectly superposed to each of the experimental data they modeled, without any adjustment of the microscopic parameters (Figure 4A). Given the number of experimental data points, the perfect match with the model, with the pre-adjustment of only two microscopic parameters, i.e., γ_{phob} and $\varepsilon_{\mathrm{mo}} - \varepsilon_{\mathrm{mm}}$, supports the validity of the theoretical approach.

Two additional features also support the validity of our model. First, at zero bilayer tension, the tensions of the droplet interfaces are the same for all the DEVs (Figure 4A), which had different geometries. This observation agrees with equation (14), which predicts in this regime that the tensions of the LD interfaces should exclusively depend on the microscopic parameters and be independent of DEV size and morphology. Second, the slope of $\gamma_{me}(\gamma_b)$ curve depends on the droplet position at zero bilayer tension (Figure 4A). The more the droplet budded inward, the steepest was the slope $d\gamma_{me}/d\gamma_b$. The exact expression of the slope $d\gamma_{me}/d\gamma_b$ at $\gamma_b = 0$ predicted by the theory is provided in supplement text, section 6.4 and, indeed, confirms that the larger θ_e at zero tension, the larger $d\gamma_{me}/d\gamma_b$.

In conclusion, the comparison of the DEV experimental data to the theory output showed a quantitative agreement, which supports the validity of our theoretical approach and its underlying hypothesis.

Discussion.

Lipid droplets have multiple biological functions that rely on the targeted proteins to their surface and their surface tension. The phospholipid monolayer of lipid droplets represents a barrier for proteins to access to lipid droplets and determine their tension (13, 14, 18, 19, 51). Since lipid droplets share a hemimembrane with the endoplasmic reticulum bilayer, at least during the steps of lipid droplet assembly (52), understanding how phospholipids partition between the bilayer and the droplet monolayer is crucial.

We developed macroscopic and microscopic models to establish the relationship between the system's free parameters composed of an oil droplet embedded in a phospholipid bilayer. We subsequently set up experiments based on droplet-embedded vesicles to test the theoretical outputs and found strong agreements. Such achievement led us to pinpoint molecular parameters or interactions responsible for the unequal phospholipid density and surface tensions between the droplet and the bilayer.

The phospholipid density discrepancy between the droplet monolayer and the bilayer in contiguity essentially pertains to the different environments underneath a PL layer in the bilayer and the droplet monolayer. For the bilayer, the PL-tails of a leaflet interact with the PL-tails of the counterpart leaflet (the interaction energy per molecule is $\varepsilon_{\mathrm{mm}}$) while in the monolayer, the PL-tails interact with the NL oil phase beneath the monolayer (the interaction energy per molecule is $\varepsilon_{\mathrm{mo}}$) (Figure 3A, C). At a constant bilayer tension, increasing $\varepsilon_{\mathrm{mm}} - \varepsilon_{\mathrm{mo}}$, for example by increasing the affinity between oil molecules and phospholipid acyl chains, will result in a phospholipid flux from the bilayer to the droplet, thereby increasing the droplet phospholipid density (Figure 4C, ρ_m). Such an improvement in phospholipid cover will induce a decrease in the droplet tension and, consequently, the spreading of the droplet, according to equation (3). Quantitatively, a 2 pN.nm variation of $\varepsilon_{\mathrm{mm}} - \varepsilon_{\mathrm{mo}}$, at fixed bilayer tension, will result in a variation in density of the order of a few percent (Figure 4D).

Should the bilayer present an asymmetry of phospholipid composition between its two leaflets, the droplet's inner and outer phospholipid monolayers may experience different interactions with oil molecules and therefore have different densities. Such an asymmetric monolayer phospholipid distribution will promote the droplet emergence to the better-covered monolayer (16).

The bilayer tension also impacts the phospholipid densities (Figure 4E). If the bilayer tension is increased, the densities of the bilayer and monolayer will decrease simultaneously. However, the relative difference between the droplet density and the bilayer density remains almost constant.

Phospholipid packing voids occur more often when triacylglycerols are infused in a bilayer (25, 27, 29, 32, 49). Such observations already suggested, at least qualitatively, that a lipid droplet connected to a bilayer would be less packed with phospholipids. This is confirmed by fluorescence measurement showing that a droplet monolayer connected to a bilayer is ~13% less packed with phospholipids than the bilayer. Our approach in this paper provided an alternative measurement of the relative phospholipid densities but, most importantly, it points to the origin of such phospholipid density gradient.

Previous experimental and theoretical studies illustrated the relevance of the surface tension difference between a lipid droplet and its host membrane (16, 17, 20, 53). This tension gap controls to a large extent the morphology of droplet, its stability and budding capacity. While the tension of organelles such as the ER is very low (34), the surface tension of LD forming in their membrane is much larger (19). This could seem surprising since the monolayers at the LD interfaces and the host membrane leaflets are connected. The present work shows how the surface tensions of the forming LD and host membrane are coupled in general and reveals the microscopic origin of the different tensions. Our results explains how a lipid droplet connected to a nearly tensionless membrane can keep a relatively high surface tension.

Finally, our theoretical approach may present two limitations. First, our model does not explicitly consider the partitioning of oil molecules from the droplet to the bilayer hydrophobic region, as seen in DEVs, which alter the membrane's biophysical properties (49). From a theoretical standpoint, it will be interesting to include the presence of these oil molecules to gain accuracy in the microscopic description. Nonetheless, the match between our theoretical predictions and experimental data, including fluorescent density measurements with DEVs (30), suggests that the oil-free description captured the dominant mechanisms controlling the phospholipid densities, as well as the interdependence between surface tensions. Secondly, in the biologically relevant tensions, below 0.1 mN/m (34), the bilayer tension mostly affects the excess area stored in the thermal undulations (54, 55) rather than the intermolecular distance between phospholipids in the bilayer. In other words, tension impacts the effective density, *i.e.* the inverse of the projected area per molecule, rather than the real surface density. This effect of thermal undulations is not included in our theoretical description, in particular in the equation of state (13) for the bilayer tension. Our model might thus be unable to precisely reproduce $\gamma_{me}(\gamma_b)$ curves (Figure 4A) for very low bilayer tension, provided such curves could be obtained experimentally in this range. However, the most important effect expected is that in the low-tension regime, the real surface density of the bilayer is always very close to the zero-tension density ρ_m^0 and then the monolayer tension close to γ_m^0 (equation 16). Then, the conclusions drawn for the zero-bilayer tension case should hold more generally in all the low bilayer tension regime.

In conclusion, our present study highlights critical parameters that may modulate the phospholipid density at the surface of lipid droplets connected to the endoplasmic reticulum. More generally, our approach may be upgraded to study how phospholipid mixtures, and even protein mixtures, redistribute or partition between the bilayer and the droplet, a crucial question in lipid droplet biology.

Declaration of Interest.

The authors declare no competing interests.

Author Contributions.

AC, LF and ART designed, performed research, analyzed data and wrote the paper.

Acknowledgments.

We are thankful to our group members for their valuable comments and critical discussions about the manuscript. This work was supported the ANR-MOBIL and ANR-21-CE11-LIPRODYN to ART.

References:

1. Thiam, A.R., R.V. Farese Jr, and T.C. Walther. 2013. The biophysics and cell biology of lipid droplets. *Nat. Rev. Mol. Cell Biol.* 14:775.

2. Walther, T.C., J. Chung, and R.V. Farese Jr. 2017. Lipid droplet biogenesis. *Annu. Rev. Cell Dev. Biol.* 33:491–510.

3. Jackson, C.L. 2019. Lipid droplet biogenesis. *Curr. Opin. Cell Biol.* 59:88–96.

4. Thiam, A.R., and E. Ikonen. 2020. Lipid Droplet Nucleation. *Trends Cell Biol.*

5. Khandelia, H., L. Duelund, K.I. Pakkanen, and J.H. Ipsen. 2010. Triglyceride blisters in lipid bilayers: implications for lipid droplet biogenesis and the mobile lipid signal in cancer cell membranes. *PloS One*. 5:e12811.

6. Choudhary, V., N. Ojha, A. Golden, and W.A. Prinz. 2015. A conserved family of proteins facilitates nascent lipid droplet budding from the ER. *J Cell Biol*. 211:261–271.

7. Salo, V.T., I. Belevich, S. Li, L. Karhinen, H. Vihinen, C. Vigouroux, J. Magré, C. Thiele, M. Hölttä-Vuori, and E. Jokitalo. 2016. Seipin regulates ER–lipid droplet contacts and cargo delivery. *EMBO J.* 35:2699–2716.

8. Thiam, A.R., B. Antonny, J. Wang, J. Delacotte, F. Wilfling, T.C. Walther, R. Beck, J.E. Rothman, and F. Pincet. 2013. COPI buds 60-nm lipid droplets from reconstituted water–phospholipid–triacylglyceride interfaces, suggesting a tension clamp function. *Proc. Natl. Acad. Sci.* 110:13244–13249.

9. Wilfling, F., A.R. Thiam, M.-J. Olarte, J. Wang, R. Beck, T.J. Gould, E.S. Allgeyer, F. Pincet, J. Bewersdorf, and R.V. Farese Jr. 2014. Arf1/COPI machinery acts directly on lipid droplets and enables their connection to the ER for protein targeting. *Elife*. 3:e01607.

10. Jacquier, N., V. Choudhary, M. Mari, A. Toulmay, F. Reggiori, and R. Schneiter. 2011. Lipid droplets are functionally connected to the endoplasmic reticulum in Saccharomyces cerevisiae. *J Cell Sci*. 124:2424–2437.

11. Markgraf, D.F., R.W. Klemm, M. Junker, H.K. Hannibal-Bach, C.S. Ejsing, and T.A. Rapoport. 2014. An ER protein functionally couples neutral lipid metabolism on lipid droplets to membrane lipid synthesis in the ER. *Cell Rep.* 6:44–55.

12. Wilfling, F., H. Wang, J.T. Haas, N. Krahmer, T.J. Gould, A. Uchida, J.-X. Cheng, M. Graham, R. Christiano, and F. Fröhlich. 2013. Triacylglycerol synthesis enzymes mediate lipid droplet growth by relocalizing from the ER to lipid droplets. *Dev. Cell*. 24:384–399.

13. Dhiman, R., S. Caesar, A.R. Thiam, and B. Schrul. 2020. Mechanisms of protein targeting to lipid droplets: A unified cell biological and biophysical perspective. In: Seminars in Cell & Developmental Biology. Elsevier.

14. Kory, N., R.V. Farese Jr, and T.C. Walther. 2016. Targeting fat: mechanisms of protein localization to lipid droplets. *Trends Cell Biol.* 26:535–546.

15. Thiam, A.R., and L. Forêt. 2016. The physics of lipid droplet nucleation, growth and budding. *Biochim. Biophys. Acta*. 1861:715–722.

16. Chorlay, A., L. Monticelli, J.V. Ferreira, K.B. M'barek, D. Ajjaji, S. Wang, E. Johnson, R. Beck, M. Omrane, and M. Beller. 2019. Membrane asymmetry imposes directionality on lipid droplet emergence from the ER. *Dev. Cell*. 50:25–42.

17. Deslandes, F., A.R. Thiam, and L. Forêt. 2017. Lipid Droplets Can Spontaneously Bud Off from a Symmetric Bilayer. *Biophys. J.* 113:15–18.

18. Thiam, A.R., and I. Dugail. 2019. Lipid droplet–membrane contact sites–from protein binding to function. *J. Cell Sci.* 132:jcs230169.

19. Ben M'barek, K., D. Ajjaji, A. Chorlay, S. Vanni, L. Forêt, and A.R. Thiam. 2017. ER Membrane Phospholipids and Surface Tension Control Cellular Lipid Droplet Formation. *Dev. Cell*. 41:591-604.e7.

20. Chorlay, A., and A.R. Thiam. 2018. An asymmetry in monolayer tension regulates lipid droplet budding direction. *Biophys. J.* 114:631–640.

21. Santinho, A., V.T. Salo, A. Chorlay, S. Li, X. Zhou, M. Omrane, E. Ikonen, and A.R. Thiam. 2020. Membrane Curvature Catalyzes Lipid Droplet Assembly. *Curr. Biol.* 30:2481-2494.e6.

22. Choudhary, V., G. Golani, A.S. Joshi, S. Cottier, R. Schneiter, W.A. Prinz, and M.M. Kozlov. 2018. Architecture of lipid droplets in endoplasmic reticulum is determined by phospholipid intrinsic curvature. *Curr. Biol.* 28:915–926.

23. Zanghellini, J., F. Wodlei, and H.H. Von Grünberg. 2010. Phospholipid demixing and the birth of a lipid droplet. *J. Theor. Biol.* 264:952–961.

24. Caillon, L., V. Nieto, P. Gehan, M. Omrane, N. Rodriguez, L. Monticelli, and A.R. Thiam. 2020. Triacylglycerols sequester monotopic membrane proteins to lipid droplets. *Nat. Commun.* 11:1–12.

25. Prévost, C., M.E. Sharp, N. Kory, Q. Lin, G.A. Voth, R.V. Farese Jr, and T.C. Walther. 2018. Mechanism and determinants of amphipathic helix-containing protein targeting to lipid droplets. *Dev. Cell*. 44:73–86.

26. Kim, S., and J.M. Swanson. 2020. The Surface and Hydration Properties of Lipid Droplets. *Biophys. J.* 119:1958–1969.

27. Kim, S., M.I. Oh, and J.M. Swanson. 2021. Stressed lipid droplets: How neutral lipids relieve surface tension and membrane expansion drives protein association. *J. Phys. Chem. B*.

28. Kumanski, S., B.T. Viart, S. Kossida, and M. Moriel-Carretero. 2021. Lipid Droplets Are a Physiological Nucleoporin Reservoir. *Cells*. 10:472.

29. Bacle, A., R. Gautier, C.L. Jackson, P.F. Fuchs, and S. Vanni. 2017. Interdigitation between triglycerides and lipids modulates surface properties of lipid droplets. *Biophys. J.* 112:1417–1430.

30. Chorlay, A., and A.R. Thiam. 2020. Neutral lipids regulate amphipathic helix affinity for model lipid droplets. *J. Cell Biol.* 219.

31. Čopič, A., S. Antoine-Bally, M. Gimenez-Andres, C.T. Garay, B. Antonny, M.M. Manni, S. Pagnotta, J. Guihot, and C.L. Jackson. 2018. A giant amphipathic helix from a perilipin that is adapted for coating lipid droplets. *Nat. Commun.* 9:1332.

32. Ajjaji, D., K. Ben M'barek, B. Boson, M. Omrane, A. Gassama-Diagne, M. Blaud, F. Penin, E. Diaz, B. Ducos, F.-L. Cosset, and A.R. Thiam. 2021. Hepatitis C virus core protein uses triacylglycerols to fold onto the endoplasmic reticulum membrane. *Traffic*. 1–18.

33. Ajjaji, D., K. Ben M'barek, M.L. Mimmack, C. England, H. Herscovitz, L. Dong, R.G. Kay, S. Patel, V. Saudek, and D.M. Small. 2019. Dual binding motifs underpin the hierarchical association of perilipins1–3 with lipid droplets. *Mol. Biol. Cell*. 30:703–716.

34. Upadhyaya, A., and M.P. Sheetz. 2004. Tension in tubulovesicular networks of Golgi and endoplasmic reticulum membranes. *Biophys. J.* 86:2923–2928.

35. Marsh, D. 2007. Lateral pressure profile, spontaneous curvature frustration, and the incorporation and conformation of proteins in membranes. *Biophys. J.* 93:3884–3899.

36. Marsh, D. 1996. Lateral pressure in membranes. *Biochim. Biophys. Acta BBA-Rev. Biomembr.* 1286:183–223.

37. Nagle, J.F. 1976. Theory of lipid monolayer and bilayer phase transitions: effect of headgroup interactions. *J. Membr. Biol.* 27:233–250.

38. Baoukina, S., L. Monticelli, M. Amrein, and D.P. Tieleman. 2007. The molecular mechanism of monolayer-bilayer transformations of lung surfactant from molecular dynamics simulations. *Biophys. J.* 93:3775–3782.

39. Hamilton, J.A. 1989. Interactions of triglycerides with phospholipids: incorporation into the bilayer structure and formation of emulsions. *Biochemistry*. 28:2514–2520.

40. Golding, M., and T.J. Wooster. 2010. The influence of emulsion structure and stability on lipid digestion. *Curr. Opin. Colloid Interface Sci.* 15:90–101.

41. Needham, D., and R.S. Nunn. 1990. Elastic deformation and failure of lipid bilayer membranes containing cholesterol. *Biophys. J.* 58:997–1009.

42. Cooke, I.R., and M. Deserno. 2006. Coupling between lipid shape and membrane curvature. *Biophys. J.* 91:487–495.

43. Lipowsky, R. 1991. The conformation of membranes. *Nature*. 349:475–481.

44. Marsh, D. 2006. Comment on Interpretation of Mechanochemical Properties of Lipid Bilayer Vesicles from the Equation of State or Pressure- Area Measurement of the Monolayer at the Air- Water or Oil- Water Interface. *Langmuir*. 22:2916–2919.

45. Pomorski, T., and A.K. Menon. 2006. Lipid flippases and their biological functions. *Cell. Mol. Life Sci. CMLS*. 63:2908–2921.

46. Anglin, T.C., and J.C. Conboy. 2009. Kinetics and thermodynamics of flip-flop in binary phospholipid membranes measured by sum-frequency vibrational spectroscopy. *Biochemistry*. 48:10220–10234.

47. De Gennes, P.-G. 1985. Wetting: statics and dynamics. *Rev. Mod. Phys.* 57:827.

48. Chorlay, A., A. Santinho, and A.R. Thiam. 2020. Making Droplet-Embedded Vesicles to Model Cellular Lipid Droplets. *STAR Protoc.* 100116.

49. Santinho, A., A. Chorlay, L. Foret, and A.R. Thiam. 2021. Fat Inclusions Strongly Alter Membrane Mechanics. *Biophys. J.*

50. Kwok, R., and E. Evans. 1981. Thermoelasticity of large lecithin bilayer vesicles. *Biophys. J.* 35:637–652.

51. Kory, N., A.-R. Thiam, R.V. Farese Jr, and T.C. Walther. 2015. Protein crowding is a determinant of lipid droplet protein composition. *Dev. Cell*. 34:351–363.

52. Henne, W.M., M.L. Reese, and J.M. Goodman. 2018. The assembly of lipid droplets and their roles in challenged cells. *EMBO J.* 37:e98947.

53. Wang, M., and X. Yi. 2021. Bulging and budding of lipid droplets from symmetric and asymmetric membranes: competition between membrane elastic energy and interfacial energy. *Soft Matter*. 17:5319–5328.

54. Helfrich, W., and R.-M. Servuss. 1984. Undulations, steric interaction and cohesion of fluid membranes. *Il Nuovo Cimento D*. 3:137–151.

55. Rawicz, W., K.C. Olbrich, T. McIntosh, D. Needham, and E. Evans. 2000. Effect of chain length and unsaturation on elasticity of lipid bilayers. *Biophys. J.* 79:328–339.

Figure Legends.

Figure 1: Equilibrium conditions of a lipid droplet connected to a phospholipid bilayer

A) Schematic view of a lipid droplet embedded in a bilayer. The two phospholipid monolayers covering the oil droplet are in continuity with the leaflets of the bilayer allowing phospholipid exchanges.

B) The mechanical equilibrium, resulting from the balance of the surface tension forces acting on the contact line, imposes the shape of the droplet reported by the two contact angles θ_e and θ_i. The bilayer tension, the external monolayer tension and the internal monolayer tension are respectively (γ_b), (γ_{me}) and (γ_{mi}).

C) Chemical equilibrium between phospholipids in the bilayer leaflet and in the monolayer. The equilibrium distribution between phospholipids in contiguous bilayer leaflet and LD monolayer is determined by the balance of their chemical potentials μ_b and μ_m. Phospholipids of a given membrane leaflet are free to exchange by lateral diffusion between the contiguous LD monolayer and the bilayer leaflet but phospholipid flip-flop is considered irrelevent. ρ_{me} and ρ_{mi} are the phospholipid density in the external and internal monolayer, ρ_{be} and ρ_{bi} are the density in the external and internal leaflet of the bilayer.

Figure 2: Experimental determination of the interdependence between surface tensions

A) Formation of the droplet-embedded vesicle (DEV) system: Giant unilamellar vesicles (GUVs) are mixed with nano emulsion droplet that are incorporated into the intermonolayer space of the GUVs to form DEVs.

B) Left, Schematic view of micropipette measurement of the monolayer surface tension of a DEV while simultaneously measuring and increasing its bilayer surface tension with a second micropipette. Right, representative confocal micrograph showing a brignthfield image of a triolein-DOPC DEV merge with the fluorescence image of the phopholipids reported by rhodamine DOPE. Scale bar is 10 µm.

C) Monolayer-bilayer surface tension diagram of a triolein-DOPC DEV. This DEV was selected with a droplet symmetrically positioned with respect to the bilayer, i.e. identical contact angles θ_e and θ_i. See supplementary figure S1A for confocal images of the experiment. See supplementary figure S1B,C for monolayer-bilayer tension diagram of DEVs with asymetric droplet position and of DEVs with other phospholipidic compositions. A trend line is drawn to highlight the linear dependence the tensions.

D) (left) Scheme of the droplet tensiometer method: an oil-in-water droplet is generated at the tip of a tube, with phospholipids added in excess in the oil phase. Compression is achieved by decreasing the droplet volume through withdrawing the oil phase. (right) Quantification of the surface tension of DOPC monolayer at triolein-buffer interface, respectively for a monolayer in continuity with a lipid bilayer with tension<0.01mN/m (DEV), a monolayer in contact with a large phospholipid reservoir disolved in the oil phase and a monolayer mechanically compressed. Data are represented as mean ±SD. Related to supplementary figures S1 D,E.

Figure 3: Microscopic description of the contiguous droplet-bilayer system

A) Microscopic contributions to the free energy density of a monolayer and of a bilayer. For the monolayer: the surface tension of the bare water/oil interface ($\gamma_{o/w}$), the interaction of the phospholipid tails with the oil phase ($f_{\mathrm{mo}} = \varepsilon_{\mathrm{mo}}\rho_m$), the lateral interaction between phospholipids (f_{int}), and the interaction of the phospholipid headgroups with water (f_{hyd}). For the bilayer: the unfavorable interactions of the PL tails with water ($f_{\mathrm{phob}} = \gamma_{\mathrm{phob}}$), the trans-interaction between phospholipid tails ($f_{\mathrm{mm}} = \varepsilon_{\mathrm{mm}}(\rho_{be} + \rho_{bi})$) of the apposed leaflet, the lateral interaction between phospholipids (f_{int}), and the interaction of the phospholipid headgroups with water (f_{hyd}).

B) Lateral pressure as a function of phospholipid density at the triolein-water interface deduced from a compression isotherm obtained from a pending droplet experiment (see supplementary Figure S2A,B).

C) Chemical potential of a bilayer and a monolayer as a function of phospholipid density. The two chemical potentials vary identically but are shifted by the amount $\varepsilon_{\mathrm{mm}} - \varepsilon_{\mathrm{mo}}$. At equilibrium a monolayer in contact with a bilayer have the same chemical potential ($\mu_b = \mu_m$) and therefore have different phopholipid densities, whose values are directily impacted by the $\varepsilon_{\mathrm{mm}} - \varepsilon_{\mathrm{mo}}$ gap.

D) Molecular structure of the different oils used to probe the effect of oil composition on monolayer-bilayer surface tension diagram.

E) Monolayer-bilayer surface tension diagram of DOPC DEVs made with different oil composition: sterol ester-triolein (1:3) (red circles), triolein (black circles) and squalene (blue circles). DEVs were selected with a droplet symmetrically positioned with respect to the bilayer. Black dot represent the average monolayer tension of osmotically deflated triolein DEVs (bilayer tension < 0.03mN/m ; n=17). Blue dot represent the average monolayer tension of osmotically deflated squalene DEVs (bilayer

tension < 0.09mN/m ; n=9). See supplementary Figure S2C for monolayer-bilayer tension diagram of squalene and sterol ester-triolein (1:3) DEVs with asymmetric positions of the droplet.

Figure 4: Validation of the microscopic model by the DEV experimental system

A) Monolayer-bilayer surface tension diagram of a triolein-DOPC DEVs having droplets with different positions relatively to the bilayer: centered droplet ($\theta_e = \pi/2$, black dots), droplet budding outward of the bilayer ($\theta_e < \pi/2$, blue dots), or droplet budding inward of the bilayer ($\theta_e > \pi/2$, red dots). See supplementary figure S3 A-D and material and methods for angle determination. Theoretical model was used to fit the centered experimental data (black line) and enabled to extract the microscopic parameters. Using the same parameters and only adjusting the droplet's size and position parameters, the model perfectly fit the data of the other DEVs with asymmetric droplet positions (blue and red lines).

B) Main microscopic parameters obtained by fitting the model to the centered experimental data.

C) Schematic illustration of the effect of the variation of ($\varepsilon_{mm} - \varepsilon_{mo}$) on phopholipid density at the surface of a droplet in contiguity with a bilayer. If the bilayer tension is kept constant, the increase $\varepsilon_{mm} - \varepsilon_{mo}$ leads to a higher density of phopholipids on the surface of the droplet and therefore a lower surface tension of the droplets which causes the droplet to spread. This can be achieved by increasing the affinity of the phospholipid tails for the oil, or decreasing the strength of the trans-interactions between phospholipid tails in the bilayer.

D) Theoretical prediction of the effect of the variation of ($\varepsilon_{mm} - \varepsilon_{mo}$) on the difference between the density of phospholipids in a bilayer sheet and that at the droplet surface. The bilayer surface tension (γ_b)) was kept at 0.5mN/m.

E) Theoretical prediction of the variation of the surface tension of the bilayer (γ_b) on the phospholipid density in the bilayer and in the monolayer of droplets. $\varepsilon_{mm} - \varepsilon_{mo}$ was kept contant at -4.4 pN.m.

Material and methods: theory.

Definition of the intensive thermodynamic quantities

The surface tension and chemical potential of a PL monolayer are defined by (supplement text, section 2),

$$\gamma_m = f_m(\rho_m) - \rho_m f_m'(\rho_m) \ , \qquad \mu_m = f_m'(\rho_m) \, , \tag{MM1}$$

where the prime denotes the derivative of the function. For each monolayer, $\gamma_{me/mi} = \gamma_m(\rho_{me/mi})$ and $\mu_{me/mi} = \mu_m(\rho_{me/mi})$. The chemical potential of a bilayer leaflet is

$$\mu_b = \partial_\rho f_b(\rho, \bar{\rho}), \tag{MM2}$$

where ρ is the density of the considered leaflet and $\bar{\rho}$ that of the opposite leaflet, so that, $\mu_{be} = \mu_b(\rho_{be}, \rho_{bi})$ and $\mu_{bi} = \mu_b(\rho_{bi}, \rho_{be})$. The surface tension of the bilayer is defined as,

$$\gamma_b = f_b(\rho_{be}, \rho_{bi}) - \rho_{be}\mu_b(\rho_{be}, \rho_{bi}) - \rho_{bi}\mu_b(\rho_{bi}, \rho_{be}) \, . \tag{MM3}$$

Materials and Methods experimental.

Preparation of GUVs.

All experiments were performed in the following HKM buffer: 50 mM Hepes, 120 mM Kacetate, and 1 mM MgCl2 (in Milli-Q water) at pH 7.4 and 275±15 mOsm.

GUVs were prepared by electro-formation. Phospholipids and mixtures thereof in chloroform at 0.5 µM were dried on an indium tin oxide (ITO) coated glass plate. The lipid film was desiccated for 1 h. The chamber was sealed with another ITO-coated glass plate. The lipids were then rehydrated with a sucrose solution (275+-15 mOsm). Electro-formation is performed using 100 Hz AC voltage at 1.0 to 1.4 Vpp and maintained for at least 1 h. This low voltage was used to avoid hydrolysis of water and dissolution of the titanium ions on the glass plate. GUVs were either stored in the chamber at 4 °C overnight or directly collected with a Pasteur pipette.

GUVs composition:

DOPC GUVs: 99 % DOPC (1,2-dioleyl-sn-3glycero-3-phosphocholine) stained with 1% Rhodamine-DOPE (1,2-dioleyl-sn-glycero-3-phosphoethanolamine-N-lissamine rhodamine B sulfonyl).

DOPA-DOPC GUVs: 30% DOPA (1,2-dioleoyl-sn-glycero-3-phosphate), 69 % DOPC, and 1% Rhodamine-DOPE.

Pufa-DOPC GUVs: 30% Pufa (18:0–20:4) (1-stearoyl-2-arach- idonoyl-sn-glycero-3-phosphocholine), 69 % DOPC, and 1% Rhodamine-DOPE.

Preparation of DEV (GUVs + oil droplet)

To prepare the oil droplets, 5 µL of the oil (triolein or squalene) was added to 45 µL of HKM buffer. The mixture was sonicated. The diameter of the resulting droplets is on the order of a few hundred nanometers. To make DEV, GUVs were then incubated with the LDs for 5 min. The GUV-LD mixture was then placed on a glass coverslip (pretreated with 10 % (w/w) BSA and washed three times with buffer).

Confocal microscope images.

All micrographs of DEV were made on a Carl ZEISS LSM 800 with X10 air objective, and observed samples were held by Glass coverslips (Menzel Glaser (24x36mm #0)).

Micromanipulation & surface tension measurements by microaspiration.

Micro-pipettes were made from capillaries drawn out with a Sutter Instruments pipette-puller. They were used to manipulate the DEVs in order to get a side view of the system. Pipettes were treated with an mPEG-Silane solution following the protocol described below.

Additionally, surface tensions were measured and modulated using the same pipettes. As shown in (Figure 2B), the micromanipulation of the external LD monolayer (or the DEV's bilayer) enables the measurement of the external monolayer surface tension (or the bilayer surface tension). Using Laplace's law and the measurement of the diameter, droplet (or bilayer) diameter, and suction pressure, the surface tension of the interface can be determined:

$$\gamma = \frac{\Delta \mathrm{Psuc}}{2\left(\frac{1}{Rp} - \frac{1}{Rd}\right)}$$

where ΔPsuc, Rp, and Rd are the suction pressure, the pipette radius, and the droplet external radius. The suction was carried out using a syringe. The resulting pressure was measured with a pressure transducer (DP103 provided by Validyne Eng. Corp, USA), the output voltage of which was monitored with a digital voltmeter. The pressure transducer (range 55 kPa) was calibrated prior to the experiments.

External monolayer and bilayer tension of DEV were measured simultaneously while increasing the bilayer surface tension to obtain the monolayer tension-bilayer tension graph shown in (Figure 2C).

Tension measurements of triolein-buffer interface covered with phospholipids

A pendant droplet tensiometer designed by Teclis Instruments was used to measure the interfacial tension of oil/water interfaces. All experiments were conducted at room temperature. DOPC phospholipids stored in chloroform were dried under argon and mixed with triolein oil. This mix was then sonicated and store at room temperature for 2h. To generate a phospholipid monolayer at the oil-buffer interface, phospholipid-in-triolein droplets (from 5 to 16.0 µl) were formed at the tip of a J-needle submerged in 5 ml of HKM buffer. The surface tension of the interface was automatically measured by the tensiometer.

Tension of an interface at equilibrium with a large reservoir of PLs dissolved in the oil phase.

Triolein was supplemented with 0.5% (w/w) DOPC to get above the critical micellar concentration. This mix was used in the pendent droplet tensiometer to form a DOPC monolayer at the oil-water interface. As the phospholipids exceeded the critical micellar concentration, the oil phase acted as a phospholipid reservoir in supplying phospholipids to the monolayer. Surface tension was measured until a plateau was reached (supplementary figure S1D). This plateau of tension is the tension designated as the tension of a monolayer connected to a phospholipids reservoir.

The tension of a mechanically compressed phospholipid monolayer.

Triolein was supplemented with 0.05% (w/w) DOPC. This mix was used in the pendent droplet tensiometer to form a DOPC monolayer at the oil-water interface. The phospholipids relocated at the oil-buffer interface resulting in a decrease of surface tension. After tension stabilization, we started to record tension while gradually sucking up the oil back in the needle. This resulted in the compression of the phospholipid monolayer at the interface, increasing of the phospholipid density and decreasing surface tension. At some compression level, a tension plateau was reached (supplementary figure

S1E). This plateau of tension is the tension designated as the tension of a monolayer mechanically compressed at its maximal PLs density.

Phospholipids monolayer characterization (DOPC).

A DOPC monolayer was formed at the triolein buffer interface using the pendent droplet tensiometer using the same condition as described in the above paragraph. After tension stabilization, the droplet area A was decreased while recording surface tension γ_m (supplementary figure S2A,B). This surface tension - droplet area isotherm is then fitted by equation (11), $\gamma_m = \gamma_{o/w} - \pi(A/N)$ with $\pi(\rho)$ given by the van der Waals equation of state $\pi(\rho) = \frac{kT\rho}{1-a\rho} - u\rho^2$ and N is the number of PL on the droplet interface. It allows deducing the values of the parameters $\gamma_{o/w}$, a, u (and N).

Determination of the contact angles between the droplet and the bilayer.

DEVs were imaged at their equatorial plane (side view). Two osculating circles are adjusted to delimit the droplet and bilayer of the DEV. θ_e, the contact angle formed by the two tangents originating from the intersection point of the two circles (see supplementary figure S3 A-D), can be determined geometrically using the following equation derived from the law of cosines:

$$\cos\theta_e = \frac{d^2 - R_g^2 - R_d^2}{2\,R_g R_d}$$

Where (R_d) is the radius of the droplet auscultating circle, (R_g) is the radius of the bilayer auscultating circle, and (d) is the distance between the two centers of the two osculating circles.

QUANTIFICATION AND STATISTICAL ANALYSIS

Statistical analysis

Unless mentioned, all values shown in the text and figures are mean ± S.D.

EQUIPMENT AND REAGENTS

Equipment: All micrographs were made on a Carl ZEISS LSM 800. Glass coverslips: Menzel Glaser (24x36mm #0). Micro-pipettes made from capillaries (1.0ODx0.58IDx150Lmm 30-0017 GC100-15b Harvard Apparatus) with a micropipette puller (Sutter instrument model P-2000). Micromanipulation (Eppendorf TransferMan® 4r). Pressure measurement unit (DP103 provided by Validyne eng. corp, USA). Plasma cleaner was purchased from Harrick Plasma (PDC-32G-2 (230V) and used at 0,8 mbar of air pressure.

Chemical product list:

Phospholipids:

DOPC (1,2-dioleyl-sn-3glycero-3-phosphocholine), DOPA (1,2-dioleoyl-sn-glycero-3-phosphate, Pufa (18:0–20:4) (1-stearoyl-2-arach- idonoyl-sn-glycero-3-phosphocholine), Rhodamine-DOPE (1,2-dioleyl-sn-glycero-3-phosphoethanolamine-N-lissamine rhodamine B sulfonyl) were from Avanti Polar Lipids (Alabaster, AL). triolein (Glyceryl trioleate T7140), Squalene (S3626), sterol-ester (C9253 1G), Hepes (54457–250-F), K acetate (P1190), MgCl2 (M8266-100G), BSA 98% (A7906-100G), and sucrose 99.5% (59378-500G) and mPEG5K-Silane (JKA3037) were from Sigma-Aldrich.

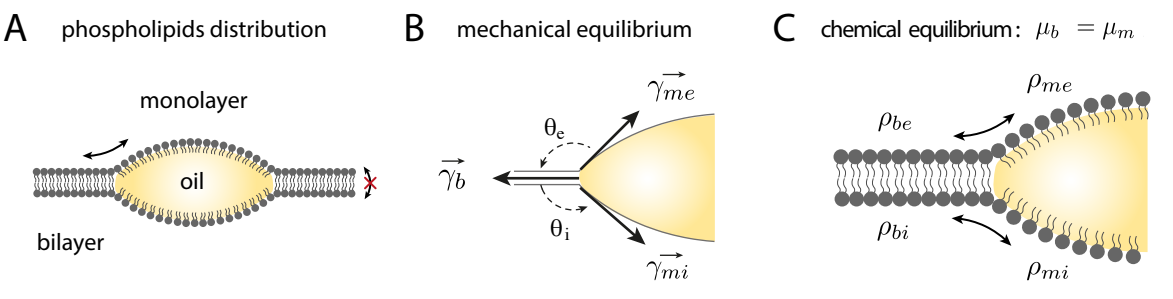
A
phospholipids distribution
monolayer
oil
bilayer
B
mechanical equilibrium
$\vec{\gamma}_{me}$
θ_e
$\vec{\gamma}_b$
θ_i
$\vec{\gamma}_{mi}$
C
chemical equilibrium: $\mu_b = \mu_m$
ρ_{me}
ρ_{be}
ρ_{bi}
ρ_{mi}

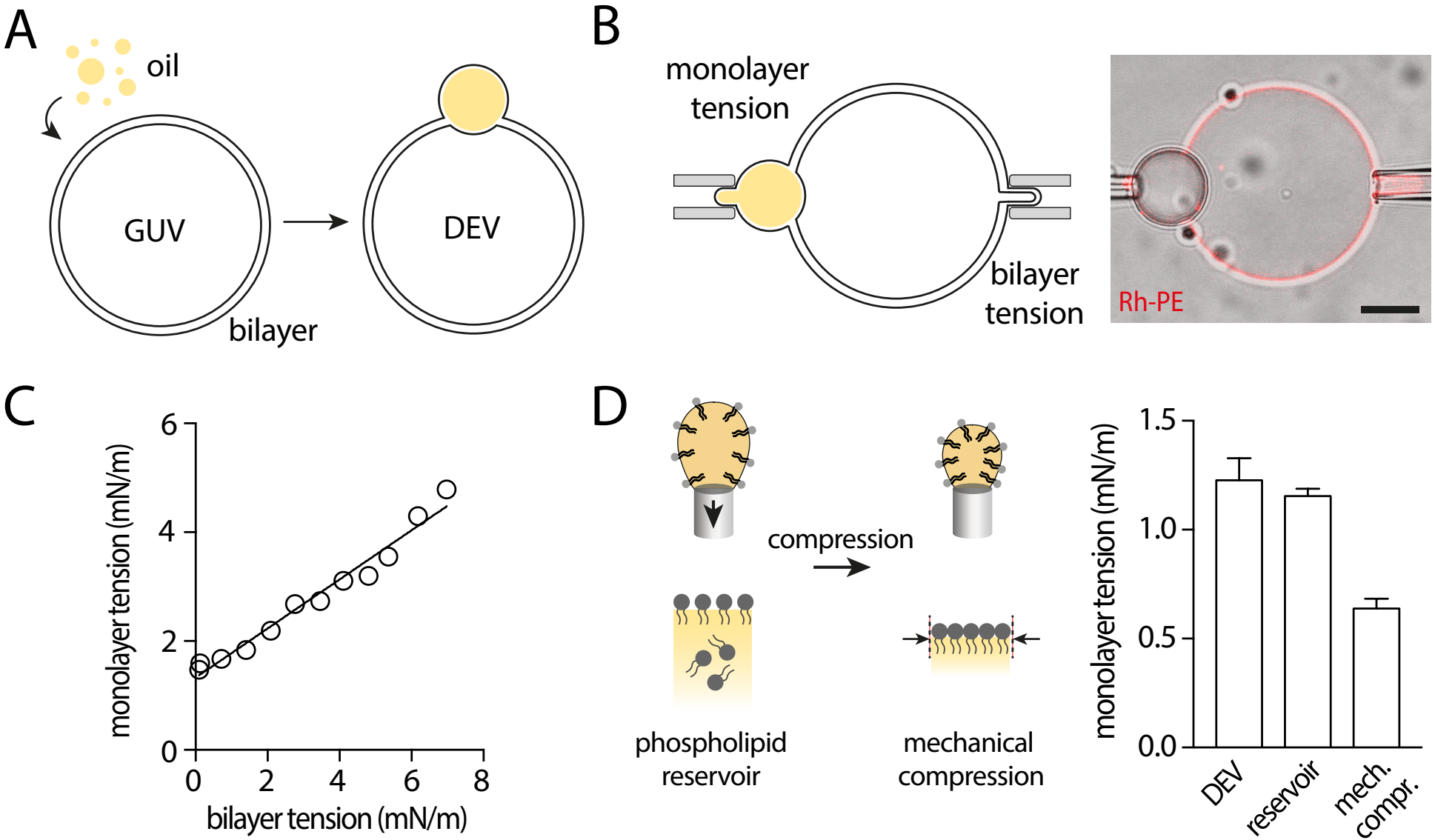
A
oil
GUV
DEV
bilayer
B
monolayer tension
bilayer tension
Rh-PE
C
monolayer tension (mN/m)
bilayer tension (mN/m)
0
2
4
6
8
D
compression
phospholipid reservoir
mechanical compression
monolayer tension (mN/m)
0.0
0.5
1.0
1.5
DEV
reservoir
mech. compr.

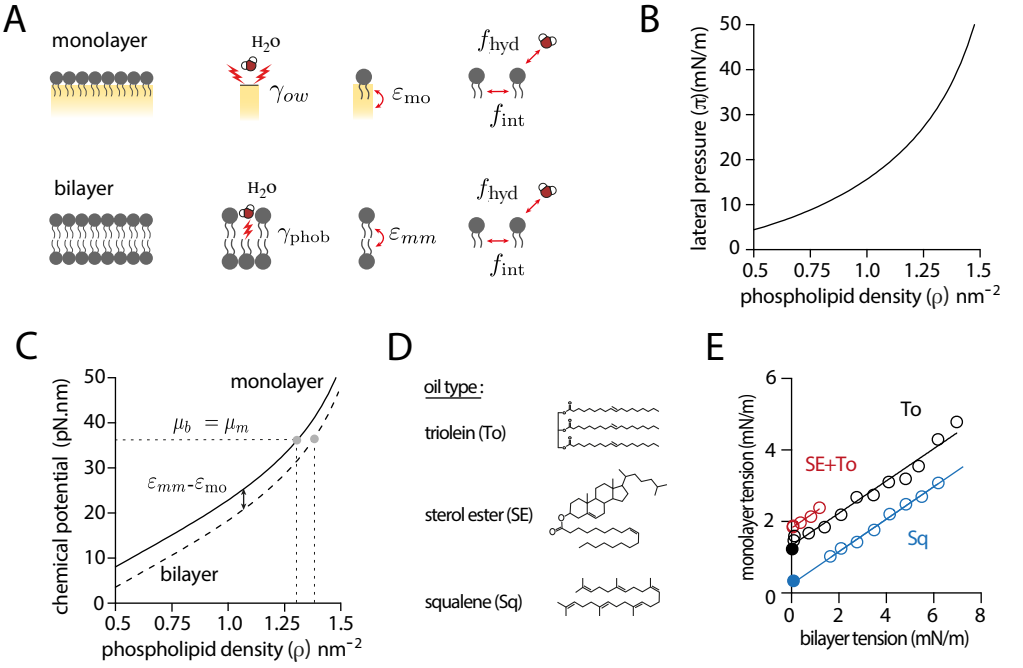
A
monolayer
H2O
γow
εmo
fhyd
fint
bilayer
H2O
γphob
εmm
fhyd
fint
B
lateral pressure (π)(mN/m)
50
40
30
20
10
0
0.5
0.75
1.0
1.25
1.5
phospholipid density (ρ) nm−2
C
chemical potential (pN.nm)
50
40
30
20
10
0
monolayer
μb = μm
εmm-εmo
bilayer
0.5
0.75
1.0
1.25
1.5
phospholipid density (ρ) nm−2
D
oil type:
triolein (To)
sterol ester (SE)
squalene (Sq)
E
monolayer tension (mN/m)
6
4
2
0
To
SE+To
Sq
0
2
4
6
8
bilayer tension (mN/m)

A

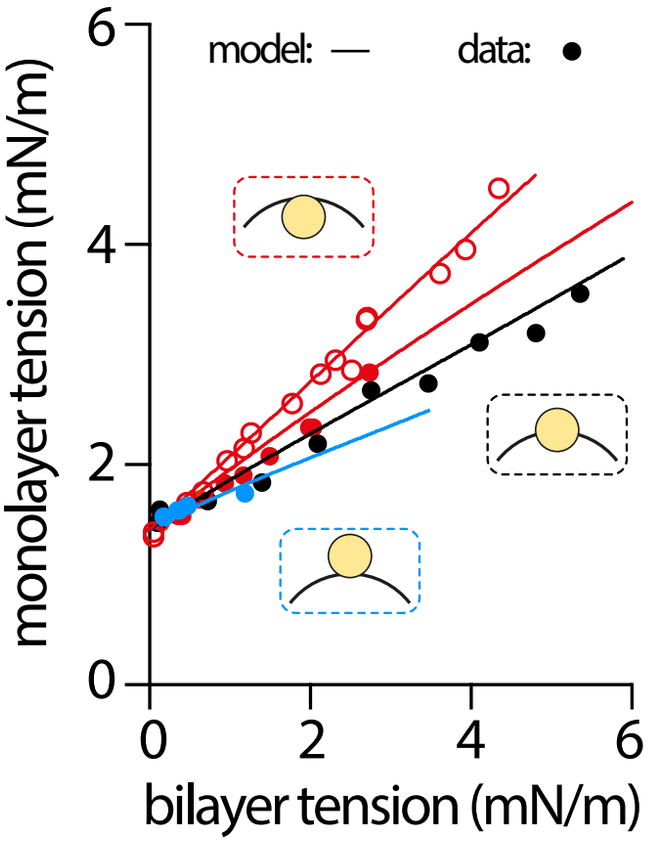

B

γ_{ow}	γ_{phob}	$\varepsilon_{mm} - \varepsilon_{\mathrm{mo}}$
34 mN/m	38.6 mN/m	-4.4 pN.nm

C

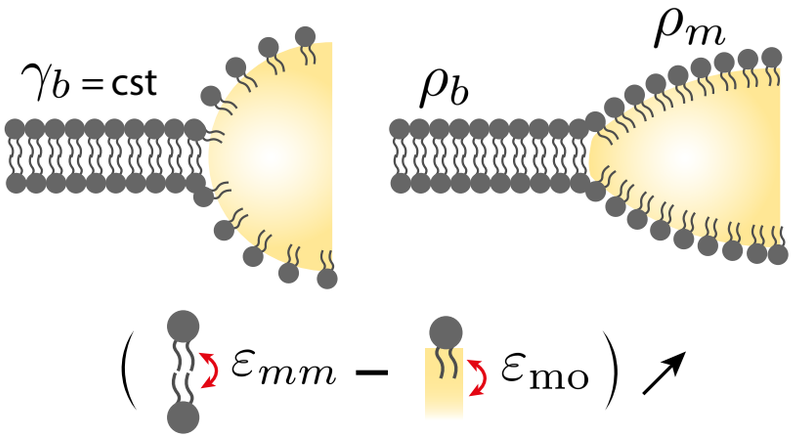

D

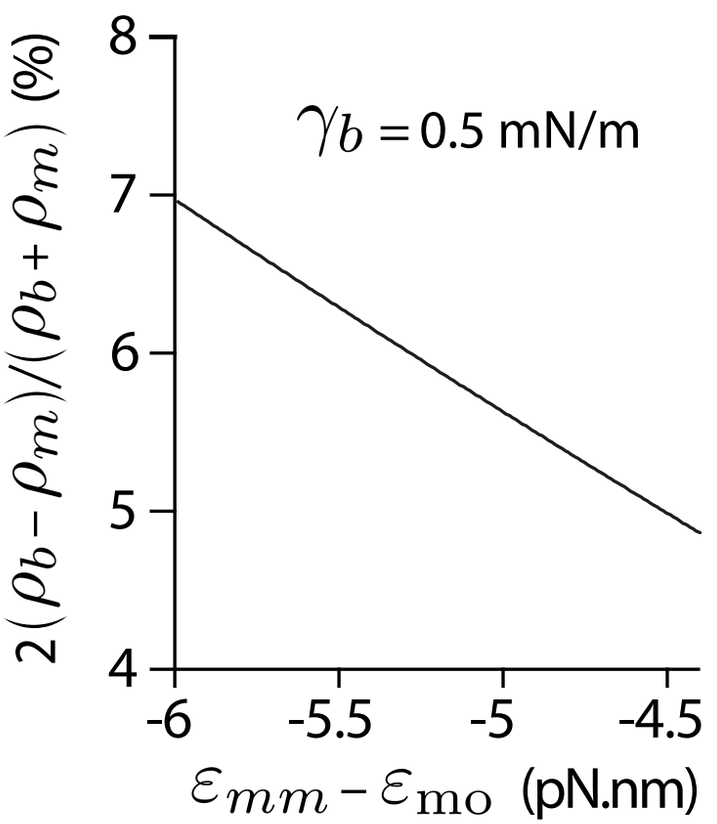

E